Dynamics of relativistic magnetized jets Report INA17_C3A24a

G. Bodo, P. Rossi
INAF Osservatorio Astrofisico di Torino
D. Mukherjee
Inter-University Centre for Astronomy and Astrophysics, Pune, India
A. Mignone
Dipartimento di Fisica, Università di Torino

1 Introduction

Relativistic jets play an important role in galaxy evolution (Fabian, 2012), they can in fact deposit energy over a large range of spatial scales, from the galactic core to the intergalactic medium (Morganti et al., 2013; Mukherjee et al., 2017). Understanding the evolution and dynamics of such jets is thus of fundamental importance for following galaxy evolution over cosmic time and requires high resolution relativisic magnetohydrodynamic simulations. These jets are observable over all the electromagnetic spectrum through their non thermal emission, either synchrotron or inverse-Compton. From the computational point of view, coupling the study of the large scale jet dynamics with the analysis of the emission properties is an extremely challenging task, since the different phenomena involve a huge range of spatial scales. Recently we have developed a new module in the PLUTO code (Vaidya et al., 2018), from which it is possible to compute the radiative properties of jets, by treating the evolution of the population of non-thermal particles by a sub-grid approach. We then initiated a systematic study of the properties, both dynamical and radiative, of high power jets. In this report we describe the first set of simulations, that are mainly focused on the dynamics.

2 Numerical setup

We investigate the propagation of relativistic magnetised jets in a stratified ambient medium. The relevant equations to be solved are the relativistic magnetohydrodynamic (RMHD) equations in a constant Minkowski metric for special relativistic flows. We assume a single-species relativistic perfect fluid (the Synge gas) described by the approximated Taub-Matthews equation of state (Mignone et al., 2005). The stratified ambient medium is maintained in hydrostatic equi-

librium by an external gravitational potential. We take a Hernquist potential (Hernquist, 1990) to represent the contribution of the stellar (baryonic) component of the galaxy, while the contribution of the dark matter component to the gravitational potential is modelled by a NFW profile (Navarro et al., 1996). No magnetic field is present in the initial configuration at t = 0 and a toroidal magnetic field is injected along with the jets. The equations are solved in a 3D Cartesian geometry with the z axis pointing along the jet direction. The resolution is such that we cover the jet radius with 10 grid points. We also followed the evolution of a passive tracer, initially set to one in the jet and zero outside, in order to follow the distribution of the jet material and its mixing with the external medium.

We perform the simulations with the PLUTO code (Mignone et al., 2007) employing the piece-wise parabolic reconstruction scheme with a second-order Runge-Kutta method for time integration and the HLLD Riemann solver (Mignone et al., 2009). The jet is injected along both positive and negative z axis from an injection region centred at (0, 0, 0). The computational box has a short extension of 1 kpc along the negative z axis. This avoids the use of a reflecting boundary condition, which may result in spurious features at the lower boundary. At all the boundaries we impose outflow boundary conditions.

The parameters defining the jet are the density contrast η between the jet and ambient density, the pressure contrast ζ_p between jet and ambient pressure, the jet Lorentz factor γ, the jet magnetization σ defined as the ratio of the Poynting flux to the jet enthalpy flux. All these parameters are defined at the injection point. The main parameters, the physical size of the computational box and the number of grid points for all the simulations are listed in Table 1. In the table we also show the jet power that can be derived by choosing a value for the jet radius and the ambient density at the injection point. We assume the jet radius to be $r_j = 100$pc in all cases except case G, H and J, where $r_j = 200$pc. The number density of the ambient gas is $n_h(r_{inj}) = 0.1$ cm^{-3} in all cases except for simulation I, where $n_h(r_{inj}) = 1$ cm^{-3}. Part of these simulations have been performed with the time allocation for the project described in this report, the rest has been performed with subsequent time allocations, that will be reported in the future.

3 Results

With this project we analysed the dynamics and evolution of relativistic jets with different initial starting parameters evolving into a hydrostatic atmosphere. We demonstrate that, depending on the jet parameters, the jet evolution is significantly affected by different MHD instabilities (Bodo et al., 1989; Mignone et al., 2010; Bodo et al., 2013; Mignone et al., 2013; Mizuno et al., 2014; Bromberg & Tchekhovskoy, 2016; Bodo et al., 2019). The type of instabilities can be broadly grouped into two categories based on jet magnetisation and power. Low power jets, with stronger magnetizations, are susceptible to current driven kink instabilities, that result in substantial bending of the jet head. In simulations with

Table 1: List of simulations and parameters

Sim.	Phys. domain (kpc)	Grid point	η_j	γ_b	σ_B	P_j (ergs^{-1})	$\mathcal{M}_j$
A	$4.5 \times 4.5 \times 10$	$288 \times 288 \times 640$	4×10^{-5}	3	0.01	1.57×10^{44}	11.5
B	$4.5 \times 4.5 \times 10$	$288 \times 288 \times 640$	4×10^{-5}	3	0.1	1.65×10^{44}	11.5
C	$4.5 \times 4.5 \times 10$	$288 \times 288 \times 640$	4×10^{-5}	3	0.2	1.73×10^{44}	11.5
D	$4.5 \times 4.5 \times 10$	$288 \times 288 \times 640$	1×10^{-4}	5	0.01	1.11×10^{45}	30.9
E[a]	$6 \times 6 \times 18$	$384 \times 384 \times 1152$	1×10^{-4}	5	0.05	1.15×10^{45}	30.9
F	$4.5 \times 4.5 \times 10$	$288 \times 288 \times 640$	1×10^{-4}	5	0.1	1.17×10^{45}	30.9
G[b]	$4.5 \times 4.5 \times 10$	$288 \times 288 \times 640$	1×10^{-4}	6	0.2	8.29×10^{45}	17.49
H	$4.5 \times 4.5 \times 10$	$288 \times 288 \times 640$	1×10^{-4}	10	0.2	1.64×10^{46}	62.77
I[c]	$4.5 \times 4.5 \times 10$	$288 \times 288 \times 640$	1×10^{-4}	5	0.1	1.17×10^{46}	30.9
J	$6 \times 6 \times 40$	$384 \times 384 \times 2560$	1×10^{-4}	10	0.1	1.51×10^{46}	62.77

[a] Simulation E is a two sided jet with the injection zone located at the centre of the domain.
[b] over-pressured jet $\zeta_p = 5$. For the rest $\zeta_p = 1$.
[c] $n_h(r_{\rm inj}) = 1$ cm^{-3}. For other simulation $n_h(r_{\rm inj}) = 0.1$ cm^{-3}.

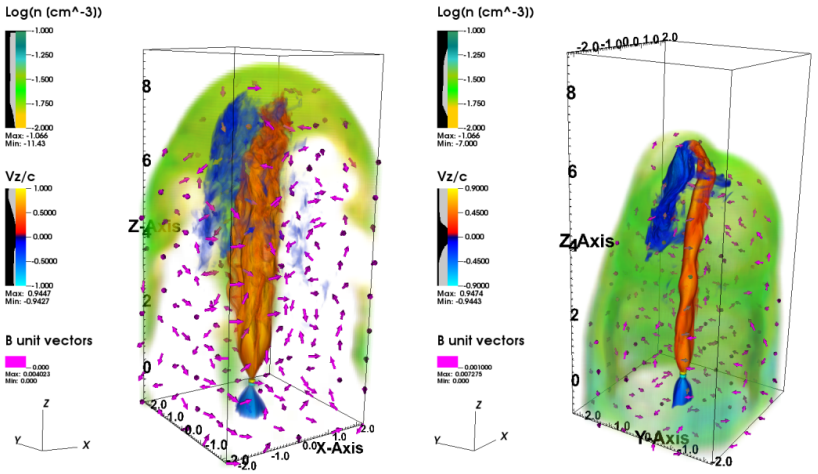

Figure 1: 3D volume rendering of the velocity in orange-blue palette with the density of the jet and cocoon in the red-green palette for simulations A (left) and B (right). The magnetic field vectors are plotted in magenta with their length scaled to their magnitude.

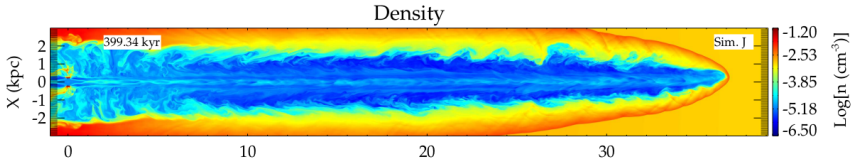

Figure 2: Density distribution in the $X - Z$ plane for simulation J.

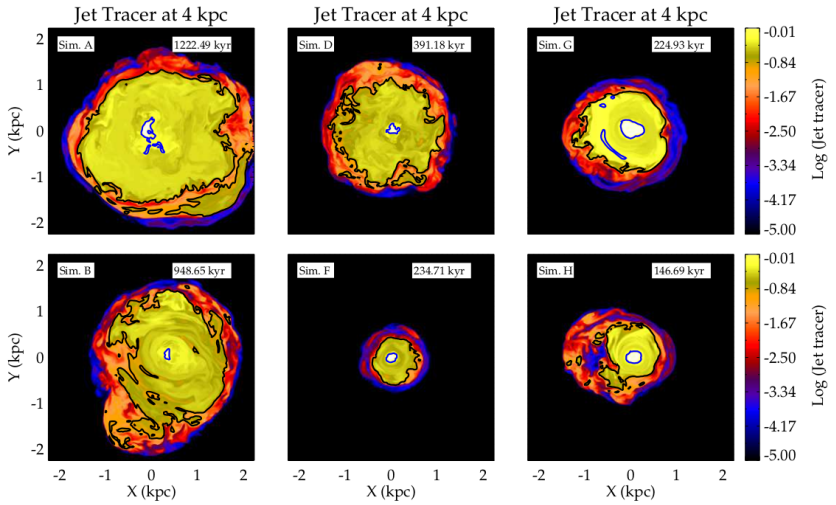

Figure 3: Cross-section of the jet tracer at a height of 4 kpc for different simulations. The blue and black contour represent jet tracer levels of 0.8 and 0.1 respectively. The top panels depict simulations where the jets are unstable to Kelvin-Helmholtz modes due to either lower magnetisation (sim. A and D) or higher pressure (sim. G), resulting in wider cross-section of the jet. Lower panels are jets where KH modes have lower growth rates with more compact jet core. Jets with stronger magnetisation have more collimated jet spine.

lower magnetization, velocity shear driven Kelvin-Helmholtz (KH) modes lead to a higher level of turbulence both close to the jet axis and in the cocoon. Such KH modes are disruptive and result in substantial deceleration of the jet with a decollimation of the jet axis. The difference between the effects of the two kinds of instabilities is shown in Fig. 1, where we show a 3D volume rendering of the velocity and of the density for cases A and B, respectively with low and high magnetizations. We see that in case A (left panel), subject to KH modes, the jet progressively decollimates, while in case B (right panel), subject to kink modes, the jet keeps its collimation, but shows signs of strong bending. In Fig. 2 we show a cut (in the $X - Z$ plane) of the density distribution for case J, that has higher power with respect to the previous cases. From the figure we can see that this jet shows very weak signs of instabilities. In Fig. 3 we show cross-sections of the jet tracer distribution for different simulations, at the same height of 4 kpc. In the top row we have cases with low magnetization, while the bottom row shows cases with high magnetization; going from left to right, the simulations have an increase of the jet power and Lorentz factor. The figure displays clearly the role of magnetic field and instabilities in determining the mixing properties for the different cases. The inner blue contour is for a value of the tracer equal to 0.8, therefore it represents the interface between the jet and the cocoon. We can see that, in the top row, the contours are more deformed than in the bottom row, in particular cases A (top left panel) and D (top middle panel) show very corrugated contours. This is indicative of the development of high m KH modes that favours mixing between jet and cocoon. The cases in the bottom row have a higher magnetization and the magnetic tension associated with the toroidal component of the magnetic field opposes the jet deformation and stabilizes high m KH modes and, correspondingly, the contours are less deformed.

The growth of instabilities has several consequences on the jet dynamics. First of all it induces a strong deceleration of the jet head advance speed, the shape of the cocoon is then very different in unstable jets, that have fatter cocoons, with respect to stable cases, that present more elongated cocoons. In addition, unstable jets tend towards a self-similar expansion where the ratio between width and length of the cocoon stays constant in time. Another consequence of the instabilities relates to the magnetic field structure. Unstable cases show a more disordered magnetic field with smaller scale structures and this may have consequences for the polarization properties of the synchrotron emission. Jets prone to instabilities have complex pressure profile at the jet head due to the motions of the jet head, which will result in multiple oblique shocks. This is in contrast to the standard model of an FRII jet with a single strong shock at the mach disc, which is often employed to calculate emission parameters and source ages. The complex shock structure with varying shock stregths will result in a wide variation of the energy distribution of the relativistic electrons being accelerated at these sites. Besides the stronger shocks at the hot spot, internal weak shocks develop inside the cocoon which may further accelerate the electrons as they flow across such shocks. Such multiple shock crossing will result in a variationof the resultant index of the power-law energy

distribution, which is usually assumed to have a single value at low energies.

The results have been obtained thanks to the time allocation through the INAF-CINECA MoU that has allowed to perform these simulations that are computationally very demanding and that necessarily require High Performance Computing resources. With this project we plan to produce a series of papers, of which the first has been already submitted and a second one is in an advanced phase of preparation:

- D. Mukherjee, G. Bodo, A. Mignone, P. Rossi & B. Vaidya, *Simulating the dynamics and non-thermal emission of relativistic magnetised jets I. Dynamics*, 2020, MNRAS, submitted
- D. Mukherjee, G. Bodo, A. Mignone, P. Rossi & B. Vaidya, *Simulating the dynamics and synchrotron emission from relativistic jets II. Emission at radio bands*, 2020, in preparation

References

Bodo G., Rosner R., Ferrari A., Knobloch E., 1989, ApJ, 341, 631

Bodo G., Mamatsashvili G., Rossi P., Mignone A., 2013, MNRAS, 434, 3030

Bodo G., Mamatsashvili G., Rossi P., Mignone A., 2019, MNRAS, 485, 2909

Bromberg O., Tchekhovskoy A., 2016, MNRAS, 456, 1739

Fabian A. C., 2012, ARAA , 50, 455

Hernquist L., 1990, ApJ, 356, 359

Mignone A., Plewa T., Bodo G., 2005, ApJS, 160, 199

Mignone A., Bodo G., Massaglia S., Matsakos T., Tesileanu O., Zanni C., Ferrari A., 2007, ApJS, 170, 228

Mignone A., Ugliano M., Bodo G., 2009, MNRAS, 393, 1141

Mignone A., Rossi P., Bodo G., Ferrari A., Massaglia S., 2010, MNRAS, 402, 7

Mignone A., Striani E., Tavani M., Ferrari A., 2013, MNRAS, 436, 1102

Mizuno Y., Hardee P. E., Nishikawa K.-I., 2014, ApJ, 784, 167

Morganti R., Fogasy J., Paragi Z., Oosterloo T., Orienti M., 2013, Science, 341, 1082

Mukherjee D., Bicknell G. V., Sutherland R., Wagner A., 2017, MNRAS, 471, 2790

Navarro J. F., Frenk C. S., White S. D. M., 1996, ApJ, 462, 563

Vaidya B., Mignone A., Bodo G., Rossi P., Massaglia S., 2018, ApJ, 865, 144